

A Signature of Chromospheric Activity in Brown Dwarfs Revealed by 2.5–5.0 μm *AKARI* Spectra

S. Sorahana^{1*} and T. K. Suzuki¹ and I. Yamamura²

¹*Department of Physics, Nagoya University, Nagoya, Aichi 464-8602, Japan*

²*Department of Space Astronomy and Astrophysics, Institute of Space and Astronautical Science (ISAS), Japan Aerospace Exploration Agency (JAXA), Sagamihara, Kanagawa 252-5210, Japan*

31 March 2021

ABSTRACT

We propose that the 2.7 μm H₂O, 3.3 μm CH₄ and 4.6 μm CO absorption bands can be good tracers of chromospheric activity in brown dwarfs. In our previous study, we found that there are difficulties in explaining entire spectra between 1.0 and 5.0 μm with the Unified Cloudy Model (UCM), a brown dwarf atmosphere model. Based on simple radiative equilibrium, temperature in a model atmosphere usually decreases monotonically with height. However, if a brown dwarf has a chromosphere, as inferred by some observations, the temperature in the upper atmosphere is higher. We construct a simple model that takes into account heating due to chromospheric activity by setting a temperature floor in an upper atmosphere, and find that the model spectra of 3 brown dwarfs with moderate H α emission, an indicator of chromospheric activity, are considerably improved to match the *AKARI* spectra. Because of the higher temperatures in the upper atmospheres, the amount of CH₄ molecules is reduced and the absorption band strengths become weaker. The strengths of the absorption bands of H₂O and CO also become weaker. On the other hand, other objects with weak H α emission cannot be fitted by our treatment. We also briefly discuss magnetic heating processes which possibly operate in upper atmospheres, by extending our numerical simulations for the Sun and stars with surface convection to brown dwarf atmospheres.

Key words: brown dwarfs – stars: late-type – stars: low-mass – stars: atmospheres – stars: chromospheres – stars: coronae.

* E-mail: sorahana.satoko@j.mbox.nagoya-u.ac.jp

1 INTRODUCTION

Brown dwarfs are objects with mass intermediate between stars and planets. No steady nuclear fusion takes place in their core, except for deuterium burning in the core of relatively massive and young ($\lesssim 10^6$ yr) brown dwarfs. Hence, they simply cool off after the initial heating by gravitational energy / deuterium burning, and thermonuclear processes do not dominate their evolution (Burrows et al. 2001). The first genuine brown dwarf, Gl 229B, was discovered by Nakajima et al. (1995), and studies of brown dwarfs are dramatically evolved in the last two decades thanks to the development of instruments and models (Tsuji 2002, 2005; Allard et al. 2001, 2003; Ackerman & Marley 2001; Cooper et al. 2003; Woitke & Helling 2003, 2004; Helling et al. 2001, 2008).

The atmospheres of brown dwarfs are dominated by molecules and dust. Many photometric/spectroscopic observations have been made in the near-infrared wavelength range shorter than $2.5 \mu\text{m}$ for studying the brown dwarf photosphere, because this wavelength range contains the spectral peaks of L dwarfs and is relatively easy to be observed. This wavelength range has features of various molecular species (e.g. TiO, VO, FeH, H₂O and CH₄) and effects of dust (e.g. Fe, Al₂O₃, MgSiO₃) extinction (Burrows et al. 2001; Tsuji et al. 1996; Tsuji 2002; Cushing et al. 2006; Helling et al. 2008). Thus spectroscopic observations in the infrared regime are the most powerful tools to obtain physical and chemical information of brown dwarf photospheres. The radiation from inner photosphere becomes weaker by the dust extinction. The effect is different between spectral types, L and T. Dust in the photosphere contributes to the spectra directly by dust extinction as well as indirectly by changing the structure of the photosphere. The effect of dust appears mainly at *J* and *H* bands in the spectra of L dwarfs (Tsuji et al. 1996; Nakajima et al. 2001). Meanwhile, the spectra of T dwarfs are less affected by the dust opacity. This indicates that the dust settles lower in the photosphere of T dwarfs. In this manner, we understand the internal chemistry and physics with near-infrared spectral data shorter than $2.5 \mu\text{m}$.

However, many critical questions related to broader wavelength range spectra remain unanswered. Cushing et al. (2008) reported that their model spectra result only poorly fits the observed spectra in the $0.95\text{--}14.5 \mu\text{m}$ for the mid- to late-L dwarfs and the early-T dwarfs. They used data observed by IRTF/SpeX ($0.9\text{--}2.5 \mu\text{m}$ and $3.0\text{--}4.0 \mu\text{m}$) and Spitzer/IRAC ($5.0\text{--}14.5 \mu\text{m}$). They concluded that the relatively poor fits at the L/T boundary, where dust contribution becomes smaller toward late type, are most likely due to the limitations of

their simple cloud model (Marley et al. 2002). In particular, the 3.0–4.0 μm range spectra resulted in the poorest fits. Observation in a wavelength range between 2.5 and 5.0 μm is difficult from the ground because of the Earth’s atmospheric effects. Therefore, little spectral data has been obtained so far.

AKARI, a Japanese infrared astronomical satellite, obtained the spectral data of this wavelength range for 27 known brown dwarfs, and we got 16 good quality data with ratio of signal to noise better than 3 (Sorahana & Yamamura 2012). They carried out the model fitting to each spectral data. They used shorter wavelength spectra (1.0–2.5 μm of IRTF/SpeX or UKIRT/CGS4; hereafter SpeX/CGS4¹) supplementary in their analysis to derive the most probable physical parameter set (effective temperature, T_{eff} , surface gravity, $\log g$, and critical temperature, T_{cr} , indicating the thickness of the dust layer) in the model fitting. By using Unified Cloudy Model (UCM hereafter; Tsuji 2002, 2005), we search for the model atmosphere that simultaneously explains both the *AKARI* and the SpeX/CGS4 spectra of each object reasonably well. However, we found that any combinations of the model parameters cannot give a reasonable fit to the observed data in the entire wavelength range (1.0–5.0 μm) of each object simultaneously, and any model spectra are always somewhat deviated from the observed spectrum in either the *AKARI* or the SpeX/CGS4 wavelength. The discrepancy implies that we are missing something important in the atmospheres of the brown dwarfs when constructing the model atmospheres.

In previous studies, X-ray, $\text{H}\alpha$, and radio emissions, which indicate the presence of high temperature regions, from some brown dwarfs (Stelzer et al. 2006; Tsuboi et al. 2003; Mohanty & Basri 2003; Schmidt et al. 2007; Reiners & Basri 2008; Berger et al. 2010; Hallinan et al. 2007, 2008). Their observations show that the $L_{\text{x}}/L_{\text{bol}}$ ratio declines with T_{eff} , where L_{x} is X-ray luminosity and L_{bol} is bolometric luminosity. However, relatively high X-ray luminosities L_{x} were observed in brown dwarfs whose spectral types are earlier than mid-L. In addition, $\text{H}\alpha$ at 6563 Å were observed (Mohanty & Basri 2003; Schmidt et al. 2007; Reiners & Basri 2008). The radio emissions from brown dwarfs were also detected (Hallinan et al., 2008). Kellett et al. (2002) and Bingham et al. (2001) proposed that the origin of radio emissions may be electron cyclotron maser emission originating in the polar regions of a large-scale magnetic field. From these observational results, the temperatures may increase somewhere in the upper atmospheres. In this paper, we call the heating region chromosphere, instead

¹ also see Section 2.2 and 2.3 for detail

Table 1. Eight Brown Dwarfs observed by *AKARI*

Object Name	Sp. Type	Instrument	References	cite of archive
2MASS J00361617+1821104	L4	SpeX	2	b
2MASS J22244381-0158521	L4.5	SpeX	1	a
GJ 1001B	L5	SpeX	1	b
SDSS J144600.60+002452.0	L5	CGS4	2	c
SDSS J053951.99-005902.0	L5	SpeX	2	b
2MASS J15074769-1627386	L5	SpeX	1	a
2MASS J08251968+2115521	L6	SpeX	2	a
2MASS J16322911+1904407	L7.5	SpeX	2	b

Reference of spectral type (1) Kirkpatrick et al. (2000), (2) Geballe et al. (2002)

The data of (a) is given from the IRTF Spectral Library by Michael Cushing, that of (b) is from the SpeX Prism Spectral Libraries by Adam Burgasser, and (c) is the data given from Dagny Looper by private communication.

of photosphere whose temperature structure follows radiative equilibrium. Thus we need to reconsider the thermal structures of brown dwarf atmospheres.

In this paper, we investigate how the broadband spectra of the observed brown dwarfs are affected by increases of the temperatures in the upper atmospheres assuming the existence of chromospheric and coronal activities. We introduce the observational data of selected brown dwarfs in Section 2. We carry out model fittings in Section 3 without (§3.1) and with (§3.2) chromospheric heating. Then, we discuss possible heating mechanism in Section 4.

2 OBSERVATIONAL DATA

2.1 The *AKARI* Sample

In this study, we focus on mid-L dwarfs from L4 to L7.5 types. The physics of early-L dwarfs may be different from brown dwarfs later than mid-L because they are placed at the threshold of hydrogen burning. On the other hand, the chromospheric activity decreases toward later type dwarfs (Gizis et al. 2000; Mohanty & Basri 2003; Berger et al. 2010). These authors statistically analyzed X-ray and H α luminosities with spectral types, and concluded that the ratio of X-ray and H α luminosities to the bolometric luminosity appears to decrease in the later spectral types. We therefore analyze the following mid-L dwarfs; 2MASS J0036+1821 (L4), 2MASS J2224-0158 (L4.5), GJ 1001B (L5), SDSS J1446+0024 (L5), SDSS J0539-0059 (L5), 2MASS J1507-1627 (L5), 2MASS J0825+2115 (L6) and 2MASS J1632+1904 (L7.5). We summarize these objects in Table 1. They are nearby and bright, thus generally well studied.

2.2 IRTF/SpeX Spectra

Almost all brown dwarfs except for SDSS J1446+0024 in our sample of this analysis have been observed by Burgasser et al. (2004, 2006, 2008, 2010); Burgasser (2007); Cushing et al. (2004) with SpeX. SpeX is the medium-resolution 0.8–5.4 μm spectrograph mounted on the NASA Infrared Telescope Facility (IRTF), which is a 3.0 meter telescope at Mauna Kea, Hawaii. The data have been obtained using its low-resolution prism-dispersed mode with the resolutions of 75–200, depending on the used slit-width for three objects, 2MASS J0036+1821, GJ1001B and 2MASS J1632+1904. We retrieve these data from the SpeX Prism Spectral Libraries built by Adam Burgasser and Sandy Leggett². Only SDSS J0539–0059 spectrum was unpublished, and we obtained from Mike Cushing (2010, private communication)³. Other three sources have been observed by SpeX using its short wavelength cross-dispersed mode (SXD) with the resolutions of 1200–2000, depending on the slit-width used. We get these data from the IRTF Spectral Library maintained by Michael Cushing⁴.

2.3 UKIRT/CGS4 Spectra

SDSS J1446+0024 has not been observed with SpeX. A spectrum in 1.0–2.5 μm of SDSS J1446+0024 was observed with UKIRT/CGS4 (Geballe et al. 2002). CGS4 is the multi-purpose grating spectrometer equipped on the 3.8 m United Kingdom Infrared Telescope (UKIRT), which is also sited on Hawaii Mauna Kea. CGS4 has four gratings. The data for SDSS J1446+0024 was observed using the 40 line/mm grating that provided the resolution of 300–2000 or $400 \times \lambda \mu\text{m}$. The spectrum was taken by adopting two broad band filters for the low and the medium resolution gratings in use with CGS4, namely B1 and B2, and the wavelength range of these filters are 1.03–1.34 μm and 1.43–2.53 μm , respectively. We get the spectral data of SDSS J1446+0024 from Dagny Looper (2010, private communication).

3 MODEL FITTING

In our previous study, we searched for the model atmospheres that explain both the *AKARI* and the SpeX/CGS4 spectra of the brown dwarfs reasonably well (Sorahana & Yamamura 2012). While the wavelength range of *AKARI* reflects the condition of relatively upper

² URL; <http://pono.ucsd.edu/~adam/browndwarfs/spexprism/html/all.html>

³ These data are now included in The SpeX Prism Spectral Libraries.

⁴ URL; http://irtfweb.ifa.hawaii.edu/~spex/IRTF_Spectral_Library/

atmospheres (Sorahana et al. 2013 in preparation), that of SpeX/CGS4 is sensitive to the inner atmosphere including the effect of dust lying in the inner atmospheres (where $\tau \sim 1$).

In this paper, we take a different fitting strategy from Sorahana & Yamamura (2012) to investigate the temperature structures of the upper atmospheres affected by the presence of chromospheres. In order to pin down the thermal structures in the inner atmospheres, we first carry out the model fittings to the only SpeX/CGS4 spectral data (§3.1.1). We call the model atmospheres determined in this way “non-heating best-fit models”. As shown in §3.1.2, none of the non-heating best-fit models shows perfect fit to the observed spectrum in the entire wavelength range. As the second step, we modify the temperature structures in the upper atmospheres assuming the presence of chromospheres/coronae and seek model atmospheres that give better fits to the observations (§3.2.1). We call the model atmospheres derived by the second step “heating best-fit models”. In Figures 1 and 2 we display the spectra synthesized from the non-heating best-fit models (*green* lines) and those from the heating best-fit models (*red* lines)⁵ in comparison with the observed spectra (*black* lines). We classify the eight brown dwarfs into two groups: In the first group consisting of three objects (Figure 1) the heating model spectra give reasonable fits to the observed spectra, while in the second group consisting of the others (Figure 2) the heating models still give poor fits to the observations (§3.2.2).

3.1 Non Heating Models

3.1.1 Fitting Procedure

We derive physical parameters of the *AKARI* objects, namely effective temperature T_{eff} , surface gravity $\log g$ and critical temperature T_{cr} by model fitting to the only SpeX/CGS4 spectral data with Unified Cloudy Model (UCM; Tsuji 2002, 2005). T_{cr} is given as an additional parameter in UCM that controls the dust dissipation thus the thickness of the dust layer. The UCM applies a simple concept with phase-equilibrium (Tsuji et al. 1996), and does not include the detail of cloud formation and growth mechanisms associated with hydrodynamic processes (Woitke & Helling 2003, 2004; Helling & Woitke 2006; Helling et al. 2008). T_{cr} cannot be determined from the physical theory but must be determined from ob-

⁵ Green lines of Figure 2 are not heating best-fit model, but heating model with f_{const} of 0.8 (see Section 3.2.1 for detail about f_{const}).

servations empirically. For $T_{\text{cr}} < T < T_{\text{cond}}$, dust condensation and sublimation are balanced. This means that the dust would exist only in the layer of $T_{\text{cr}} < T < T_{\text{cond}}$.

We follow Cushing et al. (2008) and evaluate the goodness of the model fitting to the only shorter wavelength spectra by the statistic G_k defined as

$$G_k = \frac{1}{n - m} \sum_{i=1}^n \omega_i \left(\frac{f_i - C_k F_{k,i}}{\sigma_i} \right)^2, \quad (1)$$

where n is the number of data points; m is degree of freedom (this case $m = 3$); ω_i is the weight for the i -th wavelength points (we give the equal weight as $\omega_i = 1$ for all data points because of no bias within each observed spectrum); f_i and $F_{k,i}$ are the flux densities of the observed data and k -th model, respectively; σ_i are the errors in the observed flux densities and C_k is the scaling factor given by

$$C_k = \frac{\sum \omega_i f_i F_{k,i} / \sigma_i^2}{\sum \omega_i F_{k,i}^2 / \sigma_i^2}. \quad (2)$$

G_k is equivalent to reduced χ^2 , since we adopt $\omega_i = 1$ in our analysis. This method is same with that in Sorahana & Yamamura (2012), except for fitting wavelength range.

3.1.2 Results

We show the model spectra of the non-heating best-fit models (*green* lines), which use the only SpeX/CGS4 data for the fittings, in Figures 1 & 2. We see that the non-heating best-fit models well explain the SpeX/CGS4 spectra, but the model spectra do not match with the observations in the *AKARI* wavelength range well. The principal differences between the observed and model spectra from the non-heating best-fit models are seen in the flux levels in the CH₄ at the 3.3 μm band and around the 4.0 μm region. For instance, the CH₄ bands of the three brown dwarfs, 2MASS J2224–0158, GJ 1001B and 2MASS 1632+1904, cannot be explained. The model spectrum of GJ 1001B contradictorily exhibits the CH₄ absorption feature at the 3.3 μm band, whereas it can reproduce the overall observed spectrum from 1.0 to 5.0 μm . There are also differences at 2.7 μm H₂O and 4.6 μm CO bands in the spectrum of 2MASS J2224–0158. For other four objects, SDSS J1446+0024, SDSS J0539–0059, 2MASS J1507–1627 and 2MASS J0825+2115, the entire *AKARI* spectra cannot be explained by the non-heating best-fit models especially the flux levels around 4.0 μm . The deviation of 2MASS J0036+1821 shows a different trend from other objects; i.e., the flux level around 4.0 μm in the observed spectrum is lower than that in the model spectrum, even if 2.7 μm H₂O and 4.6 μm CO bands reasonably fit well to the observation. These

Table 2. Physical Parameters of Eight Brown Dwarfs observed by *AKARI*

Object Name	Sp. Type	$T_{\text{cr}}[\text{K}]$	$\log g$	$T_{\text{eff}}[\text{K}]$	best $T_{\text{const}}[\text{K}]$	best $T_{\text{const}}/T_{\text{eff}}$	$\log(L_{\text{H}\alpha}/L_{\text{bol}})$
2MASS J00361617+1821104	L4	1800	5.5	1900	n/a	n/a	-6.26 ^a
2MASS J22244381-0158521	L4.5	1800	5.0	1700	1445	0.85	-6.48 ^a
GJ 1001B	L5	1800	5.0	1800	1260	0.70	-7.42 ^a
							-5.23 ^b
SDSS J144600.60+002452.0	L5	1700	5.0	1800	n/a	n/a	no data
SDSS J053951.99-005902.0	L5	1800	5.5	1900	n/a	n/a	no data
2MASS J15074769-1627386	L5	1800	5.5	1900	n/a	n/a	-8.18 ^a
2MASS J08251968+2115521	L6	1800	5.0	1700	n/a	n/a	-8.18 ^a
2MASS J16322911+1904407	L7.5	1800	5.5	1600	1280	0.80	-6.23 ^b

Reference of $\log(L_{\text{H}\alpha}/L_{\text{bol}})$

a: Reiners & Basri (2008), b: Mohanty & Basri (2003).

results indicate that the SpeX/CGS4 data cannot solely constrain the physical parameters of the upper atmospheres of these observed brown dwarfs.

3.2 Heating Models

3.2.1 Revising Thermal Structure

The temperature calculated from UCM as well as other models assuming the radiative equilibrium that decreases monotonically with an increasing altitude. On the other hand, some brown dwarfs exhibit activities regarding chromospheres, coronae, and flares, as discussed in §1. In such objects, the temperatures eventually stop decreasing and turn to increase somewhere in the upper atmospheres. There are several possibilities to account for the temperature inversion, which is discussed later in §4. In this section, leaving the detailed heating mechanisms aside, we adopt a very simple procedure to take into account the effect of the modified temperature structures. Since the temperature structures of the non-heating best-fit models are derived mainly from the J and H band features, which are sensitive to the effect of dust, we can reasonably assume that the temperature structures in the dust layers located in the inner photospheres are reliable even in the non-heating best-fit models. Thus we change the temperature structures only above the dust layers. We put a floor value, T_{const} , for the temperature structure of each object in the following way:

$$T(r) = \max(T(r), T_{\text{const}}) = \max(T(r), f_{\text{const}}T_{\text{eff}}), \quad (3)$$

where f_{const} is a parameter which is tuned by comparing the observed spectrum of each object (§3.2.2). In other words, the surface temperature structure is replaced with a constant value following equation 3, instead of that based on the radiative equilibrium (see also middle panel of Figure 3 for example). The gas pressure remains unchanged to keep the hydrostatic

equilibrium by reducing the density compared with the case without T_{const} , following the equation of state for an ideal gas, $p = (\rho/\mu m)kT$, where p , ρ , μ , m , k , and T are pressure, density, mean molecular weight, atomic mass unit, Boltzmann constant, and temperature, respectively. We do not take into account the inversion of the temperatures but see how the model spectra are modified when the temperatures do not decrease in the upper atmosphere. In a sense this is a minimal requirement to consider a chromosphere and/or corona. Using this heating model atmosphere, we solve the chemical equilibrium and then calculate the radiative transfer.

3.2.2 Results

We explore how the inclusion of T_{const} improves the model spectra. By varying f_{const} , we seek for the heating best-fit model for each object. We show the photosphere structure in Figure 3 for the model of $(T_{\text{cr}}/\log g/T_{\text{eff}}) = (1800\text{K}/5.0/1700\text{K})$ corresponding to the atmosphere of 2MASS J2224–0158. The top panel of this figure shows the spectra of best-fit models without (*green*) and with (*red*) heating between 1.0 and 5.0 μm . The middle panel shows the temperature structures of these model atmospheres as a function of total gas pressure. The bottom panel shows the partial pressures of each molecule versus total gas pressure. We can see that the spectral shape in the range shorter than 2.5 μm , including *J*, *H* and *K* bands, does not change significantly, but that of *AKARI* wavelength range, 2.5 to 5.0 μm , changes appreciably. From the bottom panel, we find that the CH_4 abundance in the upper region changes dramatically by introducing T_{const} . This fact is reflected in the spectral feature around 3.3 μm shown in the top panel; i.e., the absorption feature of the 3.3 μm CH_4 band is diminishing. In addition, the absorption bands of 2.7 μm H_2O and 4.6 μm CO in the heating model spectra tend to become weak. In general, the strengths of the absorption bands are a result of radiative transfer in which many factors such as number densities of molecules, excitation, velocity structure, and relation to the continuum source. Hence it is often difficult to identify a unique reason for the variation. In the current case, the higher temperature in the upper photosphere cancels the effects of increased abundance of the molecules and make the absorption even weaker.

We find that three of the eight objects, 2MASS J2224–0158, GJ 1001B and 2MASS 1632+1904, can be explained by this new treatment, but the others cannot be improved sufficiently. For the three successful objects, the best-fit values of T_{const} are 1445 K ($T_{\text{eff}} \times 0.85$), 1440 K ($T_{\text{eff}} \times$

0.70), and 1280 K ($T_{\text{eff}} \times 0.80$) for 2MASS J2224–0158, GJ 1001B, and 2MASS J1632+1904, respectively. We show the results in Figure 1 and Table 2. In the case of 2MASS J2224–0158, the non-heating best fit model cannot reproduce the *AKARI* spectrum, except for 3.8 to 4.3 μm . On the other hand, the heating best-fit model of 2MASS J2224–0158 can explain the entire observation perfectly within the error. For GJ 1001B, there is small deviation between the heating and non-heating best-fit model spectra, except for CH_4 absorption band at 3.3 μm (also see Section 3.1.2). If we consider the additional heating at upper atmosphere, the CH_4 band strength fits better to observation. Although 2MASS J1632-1904 has less S/N than the other two objects, we see that its entire spectra of the heating model fits to the observation better than that of the non-heating model.

Figure 2 shows an example of the comparison between the observations and the heating models with f_{const} of 0.8 for the other five objects. As shown in this figure, it is seen that the heating model spectra (*red*) fit better than the non-heating model spectra (*green*) especially for 4.6 μm CO band, except for 2MASS J0036+1821. However, the flux levels around 4.0 μm do not improve even in the heating model spectra. Thus, these objects with a deviation around 4.0 μm between the observation and the non-heating model cannot be explained by the modified temperature structure.

The trend of change for the revised model spectra for any stellar parameter for mid-L brown dwarfs is almost the same; i.e., only spectral features around 3.3 μm , 2.7 μm , and 4.6 μm change. In other words, the spectra shorter than 2.5 μm do not change. This is because wavelengths shorter than 2.5 μm are sensitive to the relatively inner photosphere which we do not change at all in our current analysis. As shown in Cushing et al. (2008), model fitting using narrow wavelength range spectra provide better fits than using wide wavelength range spectra at the same time. Sorahana & Yamamura (2012) analysed wide wavelength range spectra from 1.0 to 5.0 μm for model fitting to derive the most probable physical parameters for each object. They found that there are always some deviations between the observed and model spectra. For example, 2MASS J2224–0158 (L4.5), which is explained completely by our current heating model, has a large deviation at the *K* band, which is located in wavelength range shorter than 2.5 μm . Thus, when we start with the stellar parameters derived in Sorahana & Yamamura (2012), the heating model spectrum cannot reproduce the observed spectrum.

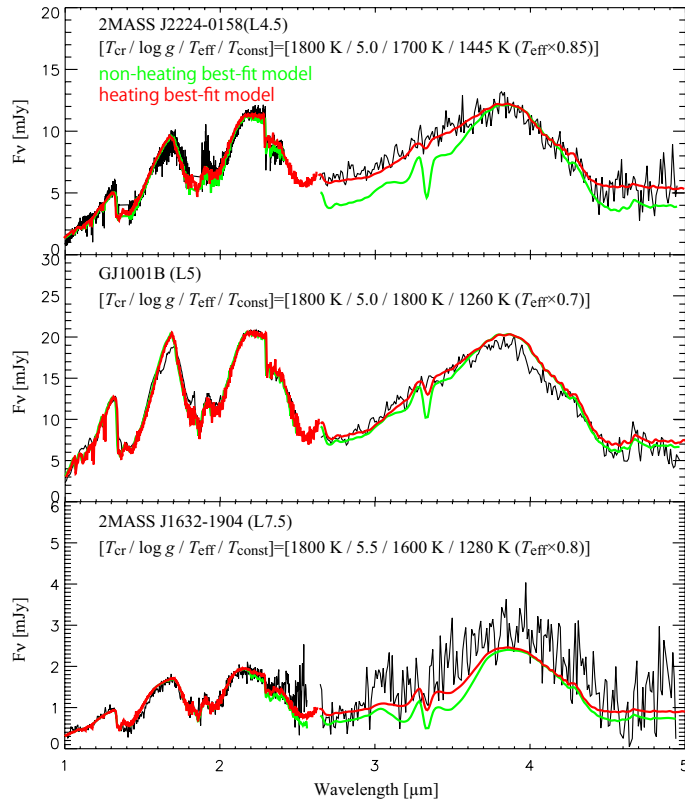


Figure 1. Comparison of the model spectra with the observed spectra for the three objects, 2MASS J2224–0158, GJ 1001B and 2MASS 1632+1904, which are well explained by the heating model atmospheres taking into account the heating in the upper atmospheres. The *black*, *green*, and *red* lines respectively correspond to the observed spectra, the non-heating best-fit model spectra, and the heating best-fit model spectra.

4 DISCUSSION

As shown in Figure 1, the model spectra of the three mid-L dwarfs are considerably improved to match the observed spectra. These models take into account the temperature floors, T_{const} , in the upper atmosphere. However, the other five objects cannot be well fitted only by including T_{const} (Figure 2). The motivation to introduce T_{const} is to minimally take into account the effect of the heating in the upper atmosphere concerning chromospheric and coronal activity. Thus it is considered that the three successful objects may have chromospheric and/or coronal activities, and the other objects do not have such strong activities. Each object could potentially be in a different state of enhanced activity, e.g., a flare, or have different effective temperatures or different ages. For example, Berger et al. (2010) discussed that X-ray luminosity decreases towards later spectral types. They suggest that this trend is caused by the dissipation of magnetic field at later spectral types. We discuss in the following section firstly from an observational side and then from a theoretical side.

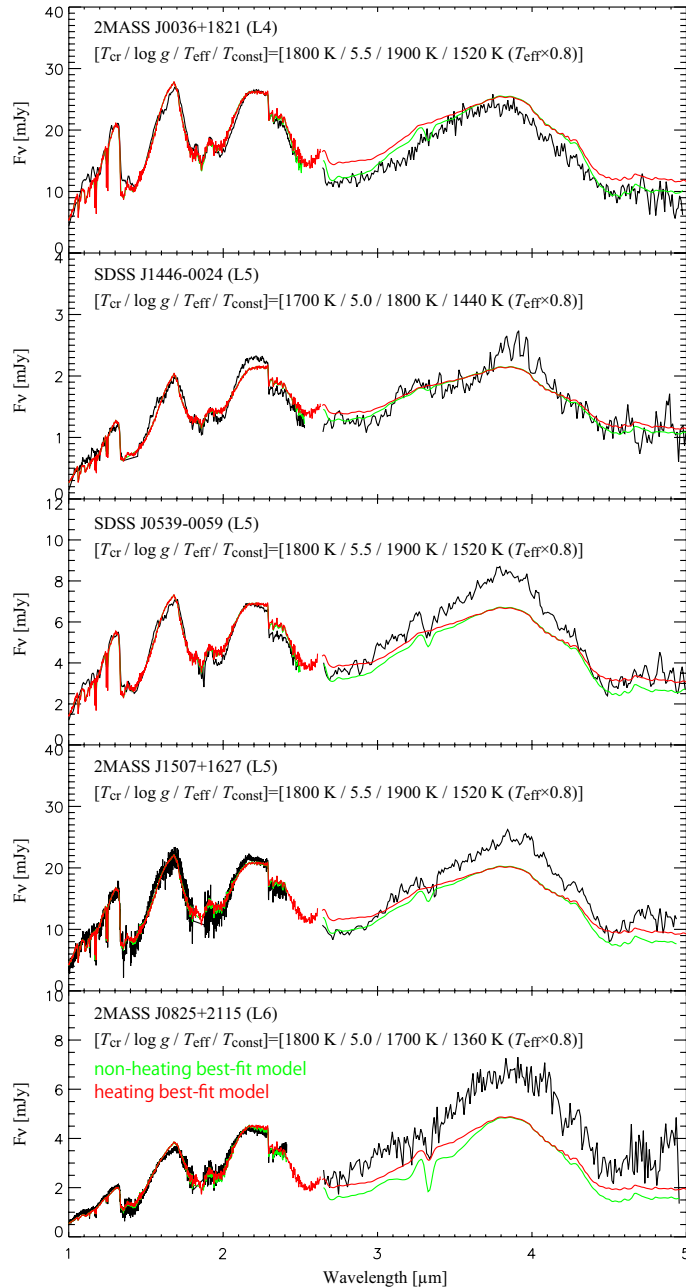


Figure 2. Same as Figure 1 but for the rest of the five brown dwarfs, 2MASS J0036+1821, SDSS J1446+0024, SDSS J0539–0059, 2MASS J1507–1627, and 2MASS J0825+2115, which cannot be well fitted by the heating model spectra.

4.1 Relation with Chromospheric Activities

X-rays (Stelzer et al. 2006; Tsuboi et al. 2003) and $H\alpha$ emissions (Mohanty & Basri 2003; Schmidt et al. 2007; Reiners & Basri 2008) are detected in some brown dwarfs. These observations suggest that at least some brown dwarfs have hot regions implicating chromospheres and/or hot coronae in their upper atmospheres. We investigate the relation between our result and observed $H\alpha$ emissions, which can be used as an indicator of chromospheric activity, of several brown dwarfs.

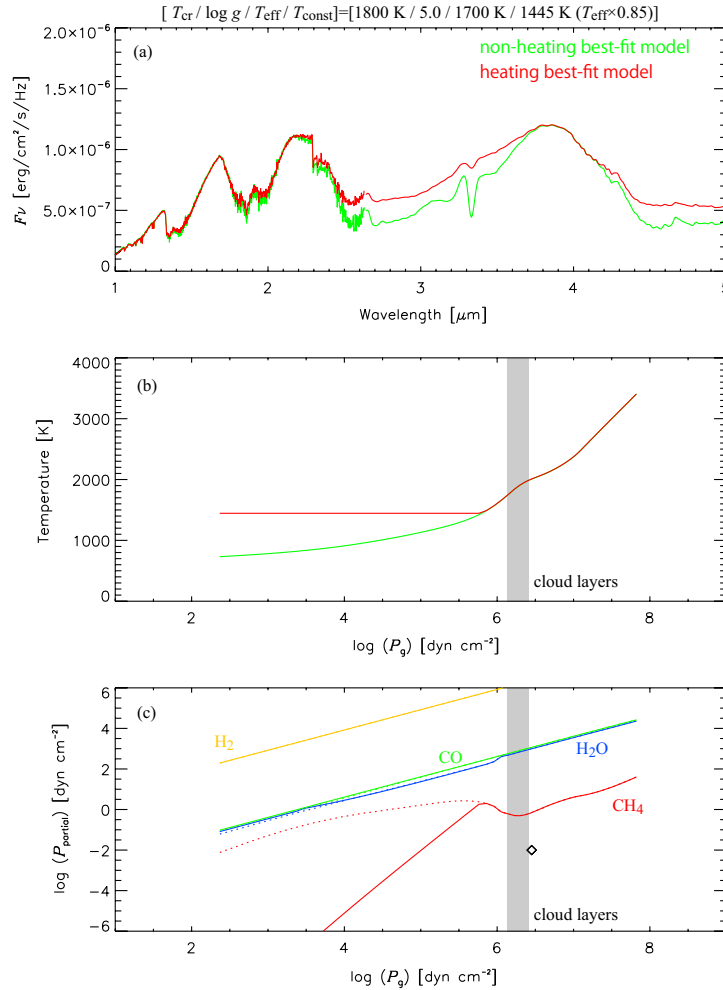


Figure 3. Comparison of spectrum, temperature and chemical structure of the L dwarf model ($T_{\text{cr}}/\log g/T_{\text{eff}} = (1800\text{K}/5.0/1700\text{K})$ for being constant lower than 1445 K ($T_{\text{eff}} \times 0.85$). (a) The spectra of the models with (red) and without (green) heating. (b) The variation of temperature from that of the non-heating model. Colors are same with panel (a). (c) Total pressure $\log P_g$ versus partial pressures of H_2 (\sim total $\log P_g$), CO, H_2O and CH_4 , which become dust, molecules, which are drawn with yellow, green, blue and red, respectively. The values of the non-heating model are drawn with dashed lines, and that of the heating model are drawn with solid lines. Grey region shows dust layers.

In Table 2 we list $\text{H}\alpha$ emission normalized by the bolometric luminosity, $L_{\text{H}\alpha}/L_{\text{bol}}$, by Mohanty & Basri (2003) and Reiners & Basri (2008); see also McLean et al. (2012) who compiled some $\text{H}\alpha$ observations including Reiners & Basri (2008). Among the eight objects, two are available in Mohanty & Basri (2003) and five are included in Reiners & Basri (2008). GJ 1001B is in the both papers. No data is available for the rest of two objects. The values for GJ 1001B in the two papers are different by two orders of magnitude. A possible explanation is that this object is very active and exhibits large time-variability related to flares. While the $L_{\text{H}\alpha}/L_{\text{bol}}$ generally decreases toward later type objects (Reiners & Basri 2008), the latest one (2MASS 1632+1904) among the eight shows rather large $L_{\text{H}\alpha}/L_{\text{bol}}$, which might be caused by high time-variability.

Among the six objects with $L_{\text{H}\alpha}/L_{\text{bol}}$, we first discuss the five objects except for 2MASS J0036+1821.

The three objects, 2MASS J2224–0158, GJ 1001B and 2MASS J1632+1904, are inferred to possess high chromospheric activity from their relatively large $L_{\text{H}\alpha}/L_{\text{bol}}$. Interestingly enough, they are the objects whose spectra are well reproduced by the heating models. On the other hand, other two objects, 2MASS J1507–1627 and 2MASS J0825+2115, which have much lower $L_{\text{H}\alpha}/L_{\text{bol}}$, cannot be explained even though the temperature floors are considered. We should consider alternative effect for these unsuccessful objects.

The final one of the six objects, 2MASS J0036+1821, with $L_{\text{H}\alpha}/L_{\text{bol}}$ appears to be an outlier. The deviation of the non-heating best-fit model spectrum from the observed spectrum appeared in 2.5 to 5.0 μm is the opposite direction from the other objects; the flux level of the model spectrum is higher than that of the *AKARI* observed spectrum. Apart from the absolute magnitude flux level, the spectral shape in the *AKARI* wavelength range itself seems to be improved, which might imply that our revised model partly makes sense in some respects in this object.

4.2 Magnetic Heating

We conclude that the additional heating in an upper atmosphere is important to understand observed spectra of brown dwarfs. So far we have not specified mechanisms that account for the heating to keep the temperatures in the upper atmospheres. The surface region of a brown dwarf is convectively unstable, and it is considered that the energy is upwardly transported by the convection (Baraffe et al. 2002; Mohanty et al. 2007). We expect that magnetic fields are generated by dynamo actions, similarly to what takes place in the Sun and stars with a surface convective layer (e.g., Choudhuri et al. 1995; Hotta et al. 2012). Various types of magnetic waves are generated and a fraction of them propagates upwardly to heat up upper regions of the atmospheres and drive the stellar winds. The Alfvén wave, among others, is a promising candidate that transfers the energy of the convection to upper regions, and leads to various magnetic activities such as chromospheres, coronae, and stellar winds, under the conditions of the Sun and other stars with surface convection. One of the authors of the present paper has studied various objects with surface convection, including the Sun (Suzuki & Inutsuka 2005, 2006; Matsumoto & Suzuki 2012), red giants (Suzuki 2007), active solar-type stars (Suzuki et al. 2013), and hot jupiters (Tanaka et al. 2013). Surface convection triggers the processes introduced here. Since brown dwarfs possess a surface convective layer, the similar processes could operate in their atmospheres. Here, we demonstrate

how the temperature structure of the model of $(T_{\text{cr}}/\log g/T_{\text{eff}}) = (1800 \text{ K}/5.0/1700 \text{ K})$ corresponding to the non-heating best-fit model for 2MASS J2224–0158 is affected by magnetic heating with a MHD (magnetohydrodynamical) simulation.

We use the same simulation code originally developed for the Sun (see Suzuki & Inutsuka 2005, 2006; Suzuki et al. 2013, for the details). We dynamically solve the structure of the atmosphere without assuming hydrostatic equilibrium. The temperature and density (accordingly gas pressure) dynamically change with time by the propagation and dissipation of waves; since Alfvén waves accompany Poynting flux, their dissipation leads to the heating of the ambient gas. We do not solve radiative transfer but use a simplified radiation cooling rate empirically determined from observation of the solar chromosphere (Anderson & Athay 1989). We also adopt the ideal MHD approximation; we assume that the magnetic field is well-coupled with the gas component. The validity of the assumption is discussed later in this subsection. We replace the Sun by 2MASS J2224–0158 as the central object. We take the mass, $M_{\star} = 0.05M_{\odot}$, as a typical brown dwarf mass, where M_{\odot} is the solar mass. We adopt the parameters of the non-heating best-fit model, $\log g = 5.0$ and $T_{\text{eff}} = 1700 \text{ K}$. The stellar radius is derived as $R_{\star} = 0.12R_{\odot}$ from M_{\star} and $\log g$. We set the inner boundary ($r = R_{\star}$) of the simulation at the top of the surface convection zone located at the position with the gas pressure $= 10^{7.08} \text{ dyn cm}^{-2}$ from our model atmosphere.

We set up an open magnetic flux tube which is similar to those on the Sun. Recent HINODE observations show that open magnetic flux tubes in coronal holes are anchored at very strong magnetic field regions with \sim kilo-Gauss (Tsuneta et al. 2008), which is nearly equipartition to the ambient gas pressure. These flux tubes open quite rapidly and the average field strength is reduced to an order of 1-10 G in the corona (Ito et al. 2010). In the present simulation for a brown dwarf, we adopt similar properties for our underlying flux tube, namely a super-radially open flux tube emanating from an equipartition kG patch.

We inject velocity perturbations at the inner boundary. In particular, transverse fluctuations with respect to the radial magnetic field excite Alfvén waves travelling upwardly. We adopt an amplitude of 20 % of the sound speed at the surface with a wide-band spectrum in proportion to the inverse of frequency ranging from period of 5 to 250 seconds, by referring to HINODE observation of the solar surface (Matsumoto & Kitai 2010); the spectrum is logarithmically centered at a period of 30 - 40 seconds, which can be scaled with $H/c_s \sim c_s/g \sim 1/10$ of the solar value ($= 5$ minutes oscillation), where H and c_s are the pressure scale height and the sound speed.

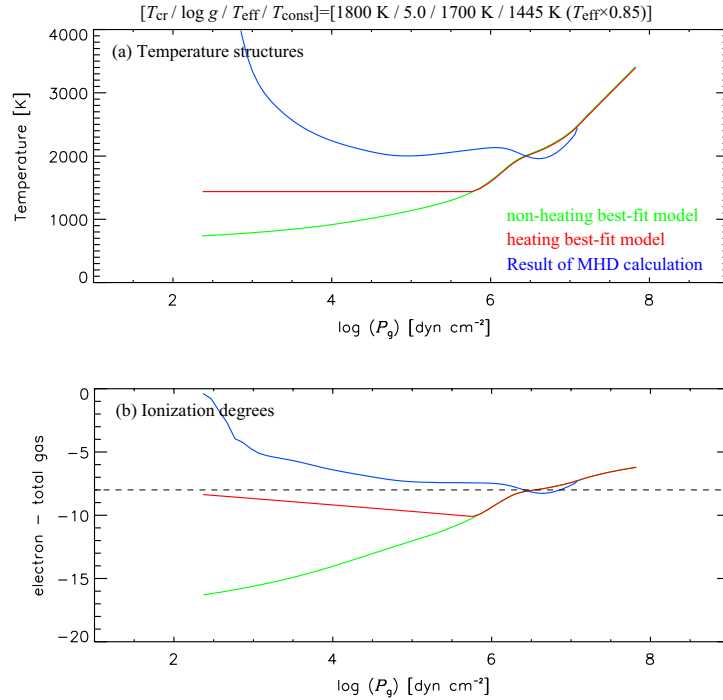


Figure 4. Comparison of (a) temperature structures and (b) ionization degrees of the non-heating best-fit model ($T_{\text{cr}}/\log g/T_{\text{eff}} = (1800\text{K}/5.0/1700\text{K})$) of 2MASS J2224–0158 (green), the heating best-fit model, and the MHD simulation (blue).

Figure 4 compares the temperature structures versus total gas pressure; the temperature derived from the simulation is averaged over sufficiently long time compared to the typical timescale of the wave propagation. The numerical simulation (blue line) shows that the temperature is nearly constant ≈ 2000 K from $p = 10^7$ to 10^4 dyn cm $^{-2}$, and rapidly increases in $p \lesssim 10^3$ dyn cm $^{-2}$. The temperature actually reaches several hundred thousand K by the heating as a result of the dissipation of Alfvén waves in the upper region. This case might be an extreme one because we are assuming the ideal MHD approximation and the more or less large velocity perturbation at the inner boundary. If the ideal MHD approximation is not satisfied, the amplitude of generated waves will be smaller because of magnetic diffusion (Mohanty et al. 2002). Injecting smaller perturbations, the numerical simulation would give lower temperature, approaching to that of the simple model with T_{const} (red line). Although our treatment of the heating models with T_{const} is quite a simple one, we expect that it could give meaningful results.

We here examine the validity of our assumption of the ideal MHD approximation for the numerical simulation. The evolution of magnetic field is determined by an induction equation,

$$\frac{\partial \mathbf{B}}{\partial t} = \nabla \times [\mathbf{v} \times \mathbf{B} - \eta(\nabla \times \mathbf{B})], \quad (4)$$

where η is resistivity. Although in our simulations $\eta = 0$ is assumed, if the second term on the right hand side dominates the first term, magnetic field is not well coupled to ambient gas and diffuses away. In the situation of a brown dwarf atmosphere, the collision between electrons and neutrals, which corresponds to the “decoupled diffusion” term in Mohanty et al. (2002), is the dominant mechanism that accounts for the resistivity. This can be expressed as

$$\eta \approx 200 \frac{\sqrt{T}}{x_e} (\text{cm}^2 \text{s}^{-1}) \quad (5)$$

(Blaes & Balbus 1994; Inutsuka & Sano 2005), where x_e is an ionization degree and temperature, T , is in units of Kelvin. By using this expression, we estimate whether the magnetic diffusion becomes significant or not.

We introduce a magnetic Reynolds number,

$$R_m = vL/\eta, \quad (6)$$

which is a nondimensional variable that measures the frozen-in condition of magnetic field; R_m is the ratio of the first term to the second term on the right-hand side of Equation (4) by replacing the rotation derivative ($\nabla \times$) via a simple division by a typical length, L . The ideal MHD condition is valid if R_m is significantly larger than unity. As a representative quantity for L , we can reasonably use the wavelength of the typical Alfvén wave we are injecting:

$$L \sim v_A \tau \sim c_s \tau = 120 \text{ km} \left(\frac{c_s}{3 \text{ km s}^{-1}} \right) \left(\frac{\tau}{40 \text{ s}} \right), \quad (7)$$

where τ is the wave period normalized by the logarithmically centered value, 40 s, and v_A is the Alfvén velocity, which is comparable to the sound speed, c_s , because we consider the equipartition magnetic flux tube. Here the normalization of $c_s = 3 \text{ km s}^{-1}$ corresponds to $T = 1500 \text{ K}$. Using Equations (5) & (7), we can estimate

$$R_m = 1 \left(\frac{v}{0.6 \text{ km s}^{-1}} \right) \left(\frac{\tau}{40 \text{ s}} \right) \left(\frac{x_e}{10^{-8}} \right) \quad (8)$$

where we normalize v by the velocity amplitude ($= 0.2c_s$) of the injected Alfvén waves near the inner boundary. This is a conservative estimate because the amplitude of the Alfvén waves is amplified as they propagate through the density decreasing atmosphere. Note also that the dependence on temperature (Equations 5 & 7) is canceled out because $c_s \propto \sqrt{T}$. Equation (8) shows that the magnetic diffusion is not so significant for low-frequency ($\tau = 40$ s) Alfvén waves, even though the ionization degree is not so high, $x_e > 10^{-8}$.

The ionization degrees of the non-heating best-fit model, the heating best-fit model, and the MHD simulation of 2MASS J2224–0158 as a function of total gas pressure are shown in

Figure 4 (b). The ionization degree of the non-heating model monotonically decreases with elevating height (decreasing total gas pressure). On the other hand, those of the heating model and the MHD simulation tend to increase, because these model atmospheres have higher temperature and lower density than non-heating model. The ionization degree of the heating model decreases with elevating height (the same as the non-heating model) until reaching the region with $T = T_{\text{const}}$, and then increases toward the upper region. The ionization degree resulting from the MHD simulation is larger than those of the other two cases and exceeds 10^{-8} in the almost entire region except for the location around $\log P_g \sim 6.5$. Therefore, the ideal MHD approximation is marginally acceptable for this case. In more elaborated studies, we should solve resistive MHD equations by using derived an ionization degree in a self-consistent manner.

In the above estimate, we only take into account thermal ionization. However, additional ionization processes are supposed to work in the atmosphere of brown dwarfs. Helling and her collaborators have proposed various ionization mechanisms, e.g. collision between charged dust grains (Helling et al. 2011,?), inter-grain electrical discharge (Helling et al. 2013), ionization by external cosmic rays (Rimmer & Helling 2013), and Alfvén ionization (Stark et al. 2013). If these processes actually work, the ionization degree will be larger than the above estimate, leading to better coupling between gas and magnetic field.

Observations show that the ratio of X-ray and $\text{H}\alpha$ luminosities to bolometric luminosity appears to decrease with later spectral type, while the ratio of radio luminosity to bolometric luminosity increase with later spectral type Berger et al. 2010; Hallinan et al. 2007 If we take into account magnetic diffusivity in our MHD simulations, we expect that the tendency of X-ray and $\text{H}\alpha$ will be interpreted at least in a qualitative sense by decreasing x_e with decreasing atmospheric temperature (Mohanty et al. 2002). In contrast, the radio luminosity is supposed to be emitted from non-thermal electrons, which is beyond the scope of our MHD simulations that handle the thermal component only.

4.3 Dust effects

For the “unsuccessful” four objects in Figure 2 excluding 2MASS J0036+1821, the flux levels around $4.0 \mu\text{m}$ differ between the observations and the model spectra. In this study, we focus the only upper temperature structure; i.e., we do not modify inner atmospheric structure affected by dust. However, the mid-L dwarfs are supposed to be most affected by

the dust in their photosphere, thus their atmospheres should be complicated. Our study shows the flux level of the 4.0 μm region is affected by dust volume (Sorahana et al. 2013 submitted to ApJ). Therefore we may need to consider some additional dust effects along with T_{cr} in UCM, for example, changing abundances, distributions, providing size distribution, and adding other dust species. Helling et al. (2008) compared five models of brown dwarf atmospheres. The other models constructed by Marley, Ackerman & Lodders, Allard & Homeier and Helling & Woitke consider vertical mixing efficiency. Yamamura et al. (2010) showed that for L dwarfs a vertical mixing in the surface of the photosphere does not affect molecular abundances in that region, thus spectral features also do not change. Grain size distributions calculated by comparing between time-scales for mixing due to convective overshooting and condensation and gravitational settling are not implemented in the UCM. We also need to consider additional effects such as hydrodynamic processes including meteorological aspects.

5 CONCLUSIONS

To solve the discrepancy between observed and model spectra between 1.0 and 5.0 μm , we consider the additional effects concerning chromospheric activity, coronae, and flares which possibly affect the temperature structure in an upper atmosphere. First, we carry out the model fittings to the only SpeX/CGS4 spectra to pin down the temperature structures in the deeper atmospheres. After that, we change the upper thermal structure in the derived model photosphere with a temperature floor, T_{const} , to take into account the effect of the chromosphere. Then we compare the heating model spectra with the observed spectra for eight brown dwarfs taken by *AKARI*. We validate that the spectrum of 2.5–5.0 μm reflects the structure of the upper photosphere; in particular, the 3.3 μm CH_4 , 2.7 μm H_2O and 4.6 μm CO bands are sensitive to the thermal structure of the upper photosphere region. From the comparison between the observed and heating model spectra, we find that three objects with relatively strong $H\alpha$ emission are consistently explained by the model spectra with T_{const} owing to the additional heating. We carry out the MHD simulation for a brown dwarf atmosphere by extending the simulation code originally developed for the Sun. The numerical simulation indeed shows that the temperature is kept nearly constant in the atmosphere and eventually increases in the upper region. Other four mid-L objects cannot be explained by our current heating model, especially the flux levels around 4.0 μm . We

may need to reconsider inner atmospheric structure with additional dust effects or some hydrodynamic processes.

ACKNOWLEDGMENTS

We thank the anonymous referee for providing critical comments and constructive suggestions to our article. This research is based on observations with *AKARI*, a JAXA project with the participation of ESA. Dr. Adam Burgasser, Dr. Michael Cushing, and Dr. Dagny Looper kindly provide us the spectral data and warm encouragement. I have greatly benefited from Prof. Ansgar Reiners. We thank to Prof. Takashi Tsuji for his kind permission to access the UCM and helpful suggestions. We also thank Dr. Takuma Matsumoto for useful discussions throughout this research, and thank Dr. Jennifer Stone for her careful checking our paper. This work is supported in part by Grants-in-Aid for Scientific Research from the MEXT of Japan, 22864006. (PI: T.K.S.)

REFERENCES

- Ackerman A. S., Marley M. S., 2001, *ApJ*, 556, 872
- Allard F., Hauschildt P. H., Alexander D. R., Tamanai A., Schweitzer A., 2001, *ApJ*, 556, 357
- Allard N. F., Allard F., Hauschildt P. H., Kielkopf J. F., Machin L., 2003, *A&A*, 411, L473
- Anderson L. S., Athay R. G., 1989, *ApJ*, 336, 1089
- Baraffe I., Chabrier G., Allard F., Hauschildt P. H., 2002, *A&A*, 382, 563
- Berger E., Basri G., Fleming T. A., Giampapa M. S., Gizis J. E., Liebert J., Martín E., Phan-Bao N., Rutledge R. E., 2010, *ApJ*, 709, 332
- Bingham R., Cairns R. A., Kellett B. J., 2001, *A&A*, 370, 1000
- Blaes O. M., Balbus S. A., 1994, *ApJ*, 421, 163
- Burgasser A. J., 2007, *ApJ*, 659, 655
- Burgasser A. J., Cruz K. L., Cushing M., Gelino C. R., Looper D. L., et al., 2010, *ApJ*, 710, 1142
- Burgasser A. J., Geballe T. R., Leggett S. K., Kirkpatrick J. D., Golimowski D. A., 2006, *ApJ*, 637, 1067
- Burgasser A. J., Liu M. C., Ireland M. J., Cruz K. L., Dupuy T. J., 2008, *ApJ*, 681, 579

- Burgasser A. J., McElwain M. W., Kirkpatrick J. D., Cruz K. L., Tinney C. G., Reid I. N., 2004, *AJ*, 127, 2856
- Burrows A., Hubbard W. B., Lunine J. I., Liebert J., 2001, *Reviews of Modern Physics*, 73, 719
- Choudhuri A. R., Schussler M., Dikpati M., 1995, *A&A*, 303, L29
- Cooper C. S., Sudarsky D., Milsom J. A., Lunine J. I., Burrows A., 2003, *ApJ*, 586, 1320
- Cushing M. C., Marley M. S., Saumon D., Kelly B. C., Vacca W. D., Rayner J. T., Freedman R. S., Lodders K., Roellig T. L., 2008, *ApJ*, 678, 1372
- Cushing M. C., Roellig T. L., Marley M. S., Saumon D., Leggett S. K., Kirkpatrick J. D., Wilson J. C., Sloan G. C., Mainzer A. K., Van Cleve J. E., Houck J. R., 2006, *ApJ*, 648, 614
- Cushing M. C., Vacca W. D., Rayner J. T., 2004, *PASP*, 116, 362
- Geballe T. R., Knapp G. R., Leggett S. K., Fan X., Golimowski D. A., Anderson S., Brinkmann J., Csabai I., Gunn J. E., Hawley S. L., et al., 2002, *ApJ*, 564, 466
- Gizis J. E., Monet D. G., Reid I. N., Kirkpatrick J. D., Liebert J., Williams R. J., 2000, *AJ*, 120, 1085
- Hallinan G., Antonova A., Doyle J. G., Bourke S., Lane C., Golden A., 2008, *ApJ*, 684, 644
- Hallinan G., Bourke S., Lane C., Antonova A., Zavala R. T., Briskin W. F., Boyle R. P., Vrba F. J., Doyle J. G., Golden A., 2007, *ApJL*, 663, L25
- Helling C., Ackerman A., Allard F., Dehn M., Hauschildt P., Homeier D., Lodders K., Marley M., Rietmeijer F., Tsuji T., Woitke P., 2008, *MNRAS*, 391, 1854
- Helling C., Jardine M., Mokler F., 2011, *ApJ*, 737, 38
- Helling C., Jardine M., Stark C., Diver D., 2013, *ApJ*, 767, 136
- Helling C., Jardine M., Witte S., Diver D. A., 2011, *ApJ*, 727, 4
- Helling C., Oevermann M., Lüttke M. J. H., Klein R., Sedlmayr E., 2001, *A&A*, 376, 194
- Helling C., Woitke P., 2006, *A&A*, 455, 325
- Helling C., Woitke P., Thi W.-F., 2008, *A&A*, 485, 547
- Hotta H., Rempel M., Yokoyama T., Iida Y., Fan Y., 2012, *A&A*, 539, A30
- Inutsuka S.-i., Sano T., 2005, *ApJL*, 628, L155
- Ito H., Tsuneta S., Shiota D., Tokumaru M., Fujiki K., 2010, *ApJ*, 719, 131
- Kellett B. J., Bingham R., Cairns R. A., Tsikoudi V., 2002, *MNRAS*, 329, 102
- Kirkpatrick J. D., Reid I. N., Liebert J., Gizis J. E., Burgasser A. J., Monet D. G., Dahn C. C., Nelson B., Williams R. J., 2000, *AJ*, 120, 447

- Marley M. S., Seager S., Saumon D., Lodders K., Ackerman A. S., et al., 2002, *ApJ*, 568, 335
- Matsumoto T., Kitai R., 2010, *ApJL*, 716, L19
- Matsumoto T., Suzuki T. K., 2012, *ApJ*, 749, 8
- McLean M., Berger E., Reiners A., 2012, *ApJ*, 746, 23
- Mohanty S., Baraffe I., Chabrier G., 2007, in Kupka F., Roxburgh I., Chan K. L., eds, *IAU Symposium Vol. 239 of IAU Symposium, Convection in brown dwarfs*. pp 197–204
- Mohanty S., Basri G., 2003, *ApJ*, 583, 451
- Mohanty S., Basri G., Shu F., Allard F., Chabrier G., 2002, *ApJ*, 571, 469
- Nakajima T., Oppenheimer B. R., Kulkarni S. R., Golimowski D. A., Matthews K., Durrance S. T., 1995, *Nature*, 378, 463
- Nakajima T., Tsuji T., Yanagisawa K., 2001, *ApJ*, 561, L119
- Reiners A., Basri G., 2008, *ApJ*, 684, 1390
- Rimmer P. B., Helling C., 2013, *ApJ*, 774, 108
- Schmidt S. J., Cruz K. L., Bongiorno B. J., Liebert J., Reid I. N., 2007, *AJ*, 133, 2258
- Sorahana S., Yamamura I., 2012, *ApJ*, 760, 151
- Stark C. R., Helling C., Diver D. A., Rimmer P. B., 2013, *ApJ*, 776, 11
- Stelzer B., Micela G., Flaccomio E., Neuhäuser R., Jayawardhana R., 2006, *A&A*, 448, 293
- Suzuki T. K., 2007, *ApJ*, 659, 1592
- Suzuki T. K., Imada S., Kataoka R., Kato Y., Matsumoto T., Miyahara H., Tsuneta S., 2013, *ArXiv e-prints*, PASJ in press
- Suzuki T. K., Inutsuka S.-i., 2005, *ApJL*, 632, L49
- Suzuki T. K., Inutsuka S.-I., 2006, *Journal of Geophysical Research (Space Physics)*, 111, 6101
- Tanaka Y. A., Suzuki T. K., Inutsuka S.-i., 2013, *ArXiv e-prints*
- Tsuboi Y., Maeda Y., Feigelson E. D., Garmire G. P., Chartas G., Mori K., Pravdo S. H., 2003, *ApJL*, 587, L51
- Tsuji T., 2002, *ApJ*, 575, 264
- Tsuji T., 2005, *ApJ*, 621, 1033
- Tsuji T., Ohnaka K., Aoki W., 1996, *A&A*, 305, L1
- Tsuji T., Ohnaka K., Aoki W., Nakajima T., 1996, *A&A*, 308, L29
- Tsuneta S., Ichimoto K., Katsukawa Y., Lites B. W., Matsuzaki K., Nagata S., Orozco Suárez D., Shimizu T., Shimojo M., Shine R. A., Suematsu Y., Suzuki T. K., Tarbell

T. D., Title A. M., 2008, ApJ, 688, 1374

Woitke P., Helling C., 2003, A&A, 399, 297

Woitke P., Helling C., 2004, A&A, 414, 335

Yamamura I., Tsuji T., Tanabé T., 2010, ApJ, 722, 682